Solid Freeform Fabrication 2016: Proceedings of the 27th Annual International Solid Freeform Fabrication Symposium – An Additive Manufacturing Conference
Reviewed Paper

Strengthening ABS, Nylon, and Polyester 3D Printed Parts by Stress Tensor Aligned Deposition Paths and Five-Axis Printing

William S. Yerazunis (*), John C. Barnwell III, Daniel N. Nikovski
Mitsubishi Electric Research Laboratories
{yerazunis, nikovski}@merl.com * - correspondence author

Abstract: *In most fused-filament fabrication (FFF) systems, all filament laydown paths are at constant Z height which creates a set of weak cleavage planes, especially in ABS plastic. To remedy this, we have designed, built, and tested a 5-axis FFF manufacturing system that accepts a CAD model, performs a finite-element model of the part as stressed in use, and for a subset of possible parts, aligns laydown paths in five dimensions (XYZ, tip, and tilt) with the in-use stress tensor; the aligned paths are then converted to 5-axis G-code and printed on our 5-axis additive manufacturing (5AAM) printer. Testing samples of a prototypical "hard to make strong" part (a hemispherical pressure tank endcap) hydrostatically shows a consistent 3-5x improvement in ultimate tensile strength, with no changes in material, design, or process parameters; the 5AAM reaches ~50% of the strength of a professionally injection molded ABS part of the same design.*

Introduction: Fused Filament Fabrication (FFF) systems generally operate by melting and extruding a polymer, placing the extrusion in a series of lay-down paths in an XY plane of constant Z. When every section of the desired part at that constant Z has been extruded, the Z motors are activated to raise the extruder a small distance (usually on the order of 0.2 to 0.5 mm) and the next set of lay-down paths is extruded.

The advantage of this mode of operation is that it is relatively simple to write the software that converts a 3D CAD model into a common format (typically the "STL", a triangular surface tesselation format), then converting the STL to layers of constant Z, and then converting the 2-D layers of constant Z into one-dimensional motion-along-a-line extruder path commands (typically in the form of G-code). At each stage of this tool chain, semi-formal or formal standards exist which make it possible to support a wide choice of different software packages and methodologies along the tool chain.

This simplicity of design has yielded a wide variety of software systems (Slic3r, Skeinforge, Cura, MatterControl, Synplify, Marlin, Teacup, etc.) and hardware for 3D FFF printing (Reprap, LulzBot, Ultimaker, Prusa, etc), many of which are completely "open source" - everything about the entire system – both hardware and software, including STL files and source code - is freely available to anyone with Internet access.

Unfortunately, this simplicity of design and partitioning of the problem into $3D \rightarrow 2D \rightarrow 1D$ causes the side effect that all volume elements at a particular level Z are filled before any volume

elements at Z+ε are filled. This means that at each Z=constant level within the final part is a possible cleavage plane, held together only by the adhesion of hot plastic extruded against solidified plastic, rather than by continuous melt.

Therein lies the problem with FFF printing- the literature reports strength variations as much as 15:1 from the injection molded or continuous melt strength along the axial fiber length versus the interlayer adhesion strength [1][2][3][4].

This high level of anisotropy has a major impact on the usability of 3D printed parts; some part designs with a tall, thin geometry are simply unprintable because the printed parts will break during removal from the print surface. Those with skill in the use (some would say “black art”) of FFF 3D printers know the importance of orienting parts during the build setup process so that they have the majority of the in-use stress is in the XY plane.

Our research agenda is to (1) reproduce and quantify the above anisotropy for a commonly useful yet weak part, (2) create strong parts with the same physical geometry as the weak parts, by aligning the strong-axis paths of lay-down extrusion with the in-use stress tensor’s maximum tension direction and (3) is to prove (or disprove) the hypothesis that it is possible to make strong parts in FFF by changing the lay-down paths so that the lay-down paths align with the direction of stress in the part.

If this hypothesis is true, the long-term goal is to optimize FFF part strength by automatically aligning the high-strength lay downs in the part with the direction of the stress tensor within the part, when the part is in actual use.

Relationship with Established Testing Methods: ASTM and other organizations publish standard testing methodologies for determining the strengths of materials. In particular, ASTM D3039 and D638 would on the face of them seem applicable to help us verify our hypothesis.

Unfortunately, both D3039 and D638 postulate that the material will be stressed linearly, and with the axial fiber length controlled to be constant with the direction of the imposed stress. This situation applies only in the case of pure tension members (which are “uninteresting”, in the sense of 3D printing, because bar and rod stock of most extrudable materials is already available at a lower price than the cost of 3D printer filament). Ahn et al [3] approaches this question by testing bars with mixed 0/90 extrusion with reasonable results, but again, this orientation would apply only in linear tension members, not in arbitrarily shaped parts.

Therefore, we decided to approach the testing problem with a specimen design that is inherently stressed in three dimensions simultaneously- a hemispherical pressure cap. The hemispherical pressure cap has a number of useful properties:

1. Hemispherical pressure caps have a simple, analytical stress tensor – the stress at any point in a thin hemispherical pressure cap is radially symmetric tension in the local plane of the cap, plus an impulse of compression from the center of the sphere.
2. Hemispherical pressure caps are a good example of a part with stresses in XY, XZ, and YZ planes in different regions of the cap, hence there is no “good” orientation to print them in and one can’t simply rotate the part to lie flat (and optimize for strength in that way).
3. Hemispherical pressure caps are a common engineering part; any manufacturing technology that claims to be “make anything” must be able to make a reasonably good pressure cap.

For the purposes of this work, we have settled on a sample fixture as shown in figure 1 (upper). The leftmost section is a 40mm thick slab of MIC6 jig plate aluminium alloy, supplied from McMaster ground flat. MIC6 jig plate alloy was chosen for it’s stability and lack of plastic compliance- MIC6 alloy literally breaks before it bends, therefore an intact jig made of MIC6 is unlikely to have been bent out of specification. The base slab bolt hole circle is on 100mm centers, and the inner edge of the O-ring groove is 41mm in diameter with the O-ring center at 45mm diameter. The central pressure port for rupture testing is 25mm in diameter and is supplied with test pressure water from a Rothenberger RP-50S hydrostatic test pump.

Figure 1: Pressure testing jig (above) and hydrostatic pressure testing pump (below)

The top retaining plate is 6mm T6061 alloy, which is far more elastic and compliant than MIC6. It carries the same bolt hole circle with eight case-hardened ¼-20 (SAE coarse) capscrews with 3/32” thick load-spreading steel washers. The capscrews are lubricated with a water resistant grease to minimize galling and corrosion. The central hole in the top plate is 40mm diameter with a ~1.5 mm radius rounding to avoid stress risers; this allows a 40mm circular test region for rupture testing. The minimum diameter to seal is approximately 45 mm, so we made our test samples 50mm in base diameter. The maximum specimen size that

will fit in the bolt hole circle is about 95mm diameter, and the capscrews can handle specimen thicknesses up to about 10 mm.

Because FFF printed specimens are not watertight, we consistently used a thin latex rubber membrane 0.5mm thick between the FFF specimen and the lower pressure test assembly. Testing with the membrane alone showed it could retain less than 0.05 MPa of pressure unassisted and we therefore ignore any effect it may have hereafter.

After testing numerous samples, we noted that rupture of domes almost always occurs by simultaneous failure of nearly the entire periphery of the dome (unlike flat disks, which fail along linear tracks or with T-shaped fractures, generally centered on the disk). We back-calculated the tension at this typical peripheral rupture location given the measured cross section and known internal pressure. Although these rupture pressure tests should not be considered equivalent to the ASTM testing methods, the stress at the time and place of rupture for our dome samples can be calculated. We found that the ratio is roughly 1:3 – that is, 1 MPa gauge pressure on our tester was approximately the same actual specimen stress as would be indicated by 3MPa stress in the ASTM D3039 protocol.

Design of Test Specimens: As noted above, we chose a hemispherical pressure cap instead of a more conventional test bar or rod because we desired a part that could not simply be rotated to be stressed in parallel with the extrusion lay-down, and because a hemispherical dome, pressurized on the inside, is a commonly used engineering part.

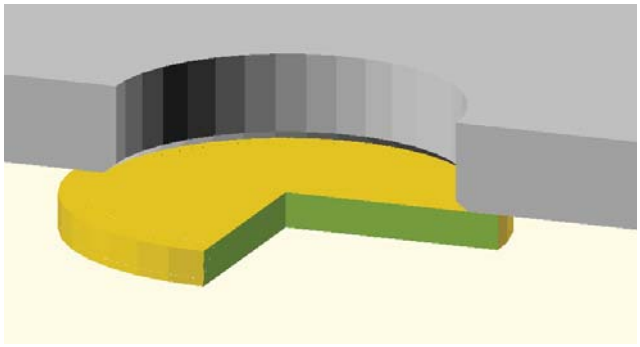

Figure 2: Control specimen: disk 50mm diameter, 4mm thick

Our “control” specimen is a simple flat disk, 50mm in diameter, and 4mm thick. This disk is a baseline disk and is an example of a part with no forces being directly placed on the Z layer bonding. The Z-forces experienced are all induced by the shear and bending of the disk during pressure testing.

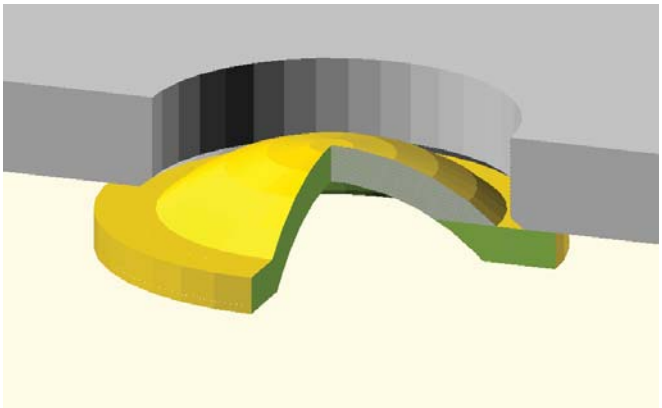

Figure 3: Experimental specimen- CAD model

The experimental specimen design begins with the same flat disk, 4mm thick, with the center domed up and a 5mm flat clamping area along the periphery. This can be achieved in OpenSCAD by a dome of 28mm outside diameter, 24mm inside diameter with the

two domes centered on a point 17mm below the lower surface; when actually printed, this yields a dome nominally ~40mm in diameter on the upper surface, and an open dome nearly 40mm on the lower surface (the quadrilateral mesh representations of these steeply sloped surfaces are a good example of where a CAD model measurement does not match well with the 3D printed results, with a deviation of where the slope changes close to 1mm between the CAD model and the actual printed objects.). Incidentally, the above design also yields a base-to-dome angle of very close to 45 degrees, which we considered to be a useful feature as many commercially made nozzles will function as designed at up to a 45 degree angle without striking the workpiece.

Our experimental specimens are made in two styles: the first style is the classic 3D print, with each Z-layer completely printed before the next Z layer is added. This is how almost every 3D printer currently in existence works. Comparing the rupture pressure of this conventionally printed 3D dome experimental specimen versus the flat disk control specimen verifies the observation that Z bonding is weak, and gives us a quantitative value of that weakness.

The second style of experimental specimen is the 5-axis additive manufacturing (5AAM) specimen as shown in figure 4. In this type of specimen, we first thin the original 4mm dome down, and then add four layers of material in the 5-axis mode. The 5AAM layers alternate between constant X (that is, a layer where the lay downs have only varying Y and Z) and constant Y (where the lay downs have only varying X and Z). These layers are made of the same polymer from the same spool, applied by the same machine at the same temperatures as the control specimens and “conventional” (first style) experimental specimens. During the extrusion of these four additional layers the A and B angles of the platform are continuously altered, so the extruder nozzle remains substantially perpendicular to the local surface slope during extrusion.

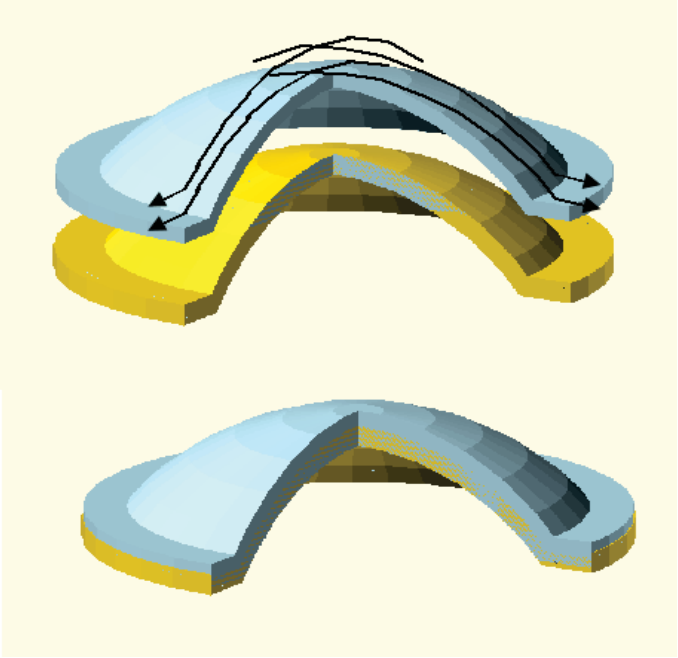

Figure 4: Experimental specimen - 5AAM version. Lower layers (yellow) are printed sequentially with planar Z. Upper layers (blue) are printed in planar X or planar Y.

Comparison of these 5AAM specimens versus the conventional 3D printed specimens will give us a qualitative answer to whether aligning the lay-down paths with the stress tensor actually can yield stronger 3D printed parts, and if so, by how much. At the worst case, the relative slopes of the 5AAM lay downs versus an “ideal” lay-down (which is unachievable, given the local radially

symmetric stress tensor in a hemispherical pressure cap) deviates only by ~10 degrees (the included angles between alternate fiber layers are 80 degrees and 100 degrees, rather than the ideal 90/90 orientation.

Experimental 5 Axis Printer Configuration: To test our hypothesis, we constructed a full-size 5-axis 3D printer, as shown in figure 5. The overall system stands about 215 cm (7 feet) tall, with a working volume of the delta positioning system of about 30 x 30 cm, and a usable Z excursion of about 50 cm. The tip-tilt platform within it uses the bottom 20cm of height, and the actual buildable volume is about 10 cm x 10 cm x 7 cm. A custom solid copper nozzle assembly with an included angle of 14 degrees from the axis of the nozzle to the maximum outside excursion, heated directly by a wrapped nichrome wire, allows the printer to print as close as 15 degrees to the vertical, although the tip-tilt platform itself is limited to +- 60 degrees per axis due to the current home switch implementation.

Mechanically, the delta robot uses three Kehling KL17H-248 stepper motors driving four-start trapezoidal profile lead screw with zero-backlash spring-loaded follower nuts, running on open-V rails. The same open-V rails are the vertical structural members. The moving delta platform is supported by six carbon-fiber arms with RadioActive RC vehicle ball joints and carries the hot end on a three-sphere, three-ring kinematic magnetic breakaway.

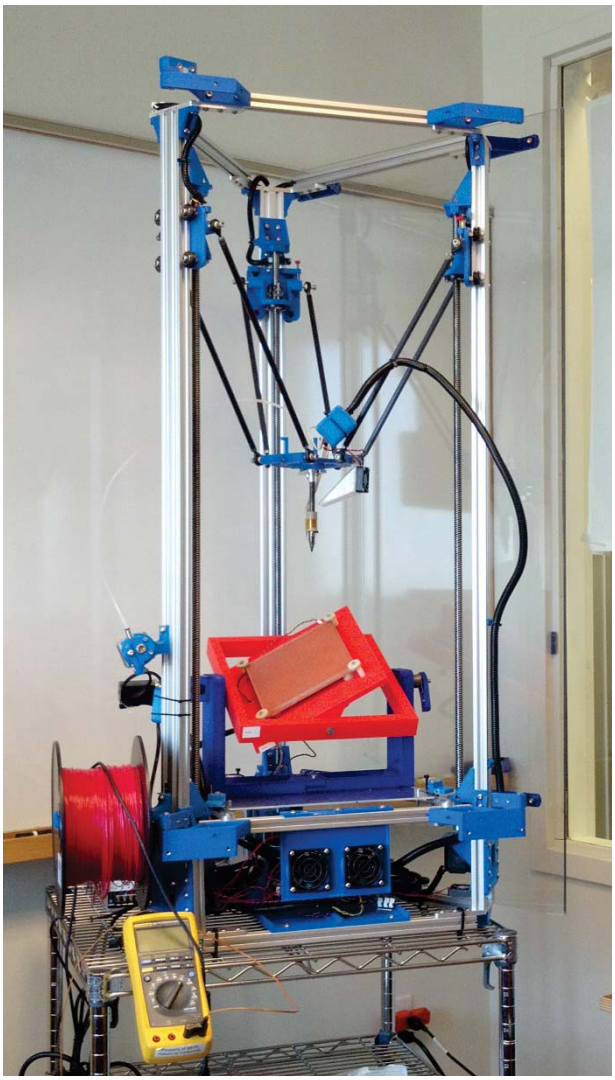

Figure 5: the five-axis printer

The tip-tilt platform was itself 3D printed in PLA on a Lulzbot TAZ printer, and is directly driven by a pair of Kysan 1040215 gearhead stepper motors via integrated 51:1 planetary stepdown gearboxes. As designed, with 10mm / turn screw pitches, 200-step steppers, and 16x microstepping, the machine has a theoretical baseline positional addressability on the order of 3 microns linearly and 38 micro-radians in tip and tilt; the actual repeatability we experience with all axes in operation and with appropriate preloads on the rotary stages is about 10 to 25 microns.

As constructed, the system uses six channels of stepper motor (three for the delta positioning

platform, two for the tip-tilt table, and one for the extruder). An additional channel of PWM is used for the cooling fan, and two channels of on-off control operate the extruder heater and the build plate heater. An Azteeq X3 Pro arduino-compatible control board equipped with six stepper-motor drivers controls all axes simultaneously.

Because none of the standard open-source 3D printer controllers support two additional axes simultaneously with motion in X, Y, Z, and E (extruder), we created our own custom software from the ground up. The controller software accepts standard G-code and allows simultaneous coordinated motion interpolated via linear interpolation for all six axes. Since the G-code (and the handshake protocol for serial transmission of the G-code) adheres to both the EIA standard and the de-facto RepRap standard, we can use common 3D printer control programs such as Pronterface to drive the 5-axis printer via USB serial line emulation (fortunately, all of the RepRap-oriented software we've encountered is willing to pass through our tip-tilt A and B motions unchanged.)

Although the home switches for the three delta screws are at the top of the towers, the machine's "zero" position is with the platform horizontal in tip and tilt (set by opto-interruptor) and the nozzle just barely touching the center of the build platform (which is 40mm above the center of rotation of the tip and tilt axes. The controller homing process raises the delta motion platform before rotating the tip-tilt table, to avoid possible table/hot end crashes. Additional protection against damage during a crash is afforded by a kinematic mount holding the extruder to the delta platform; three chromed steel precision balls are held against three nonmagnetic stainless steel rings by neodymium magnets; if forces exceed about 10 newtons, the balls pop free and release the extruder mount from the delta platform.

The firmware loaded into the printer's controller is cognizant of the particulars of the machine, such as the forward kinematics of the A and B axes, the elevation of the build platform, etc, and will maintain the same relative position of the nozzle with respect to build table X, Y, and Z during motion in A and B. This has several useful features:

- Sending a G28 (home all axes) puts the table flat and the nozzle at maximum height (giving the best possible access for maintenance of the system)
- Sending a G28 (home all axes) followed by X0 Y0 Z2.0 A0 B0 moves the hot end nozzle to 2.00 mm above the heated bed, which is ideal for checking machine calibration with a wedge style gap gauge (eg a Starrett No. 270)
- Sending a G28 (home all axes) followed by any "normal" (non-5AAM) G-code file will 3D-print that part as though the machine were a standard three-axis 3D printer (albeit one with a relatively small build area). Thus, we can do proper "control specimen versus experimental specimen" testing to compare 5AAM against standard 3D printing.

The system in full 5-axis G-code driven operation can be seen in figure 6. The system interpolates all axis motion in build table coordinates (thus a commanded rotation in A, B, or both such as G01 A10.0 B10.0 ; G01 A-10.0 B-10.0 yields a final position with the nozzle tip in the same position relative to the table and only the nozzle angle has changed. However, the motion is not linearly interpolated in table space, but rather in linear axis position space. Thus, depending on the initial and final positions, the nozzle tip may temporarily move away from the designated relative position during an angular multi-axis move or a move in delta space.

Figure 6: 5AAM machine in operation, showing coordinated motion of all five axes including local control of the nozzle perpendicular.

The magnitude of this nonlinearity is nontrivial; moving from [0,0,0] to [50,0,0] actually causes the nozzle tip to go about -1mm below the commanded line in the center of the motion. Rather than increase the computational load on the Arduino by doing the large numbers of the trigonometric calculations needed to remedy this at stepping-motor rates, we pre-process the G-code so that motions that might cause this deviation are broken into a series of shorter motions with precisely achieved endpoints, so if accuracy is critical, we can drive the deviation from perfect kinematics to well below any desired error threshold.

5-Axis G-Code Generation: To allow initial testing we first created a tool suite based on open-source 3D→2D slicers (in particular “Slic3r” but this is not a hard dependency), and then process the resulting G-code to break any large motions that might cause an accuracy violation into a series of shorter steps along the path. At this point, the resulting G-code is still executable on any 3D printer.

Our tool suite then allows us to convert the G-code into a space-filling 4DOF (X,Y,Z,Extruder) curve, rotate that curve on any axis, overlay a contoured layer in constant direction over the space-filling curve’s volume, strip away or consolidate axis motions, correct extruder motions, convert the curve back to legitimate G-code, etc. These actions “compose” (in the mathematical sense) so that it is relatively easy for a human to exercise a high level of control over the 5AAM G-code production. In situations where the part is not severely curved and the stress tensor of the part in use is analytic (or relatively simple, such as in the case of the hemispherical cap) we have a script that can automatically do the work and produce runnable 5AAM G-code suitable for our 5AAM printer.

Of course, our long range goal is to make the process work with non-analytic (i.e. FEM-derived) stress tensors, and work in that area is in process at this writing. However, even the simple

analytic script with manual overrides is sufficient to verify our critical hypothesis: that alignment of lay-down path with stress tensor yields an increase in strength.

This is an important step; without that verification, any alignment software we might create would simply be useless.

Experimental Results I : After running a significant number of "debugging" parts to verify our tool chain and 5AAM process as being relatively stable and repeatable. we proceeded to print test samples and take data.

Table 1: ABS copolymer rupture strengths:

ABS FILAMENT, SPECIMEN SHAPE	**ABS Flat disk (minimal Z stress)**	**ABS Conventional dome (full Z stress)**	**ABS 5AAM Dome (full Z stress)**
Average Rupture Pressure in MPa	**2.09 MPa**	**0.97 MPa**	**3.38 MPa**
Individual Specimen Rupture Pressure in MPa	1.8 1.95 2.0 2.2 2.3 2.3 $\sigma^2 = 0.03$	0.45 0.75 0.95 1.0 1.25 1.5 $\sigma^2 = 0.07$	2.7 2.8 2.95 3.05 3.2 3.7 3.75 3.9 3.9 $\sigma^2 = 0.21$
Strength/weight ratio in MPa / gram	0.298	0.136	0.606
5AAM advantage in Z strength			**4.45 x stronger**

Note that all of the parts are run from the same initial CAD model in OpenSCAD, made from the same spool of red 1.75mm ABS polymer (sourced from JustPLA), printed on the same printer, with the same extruder temperature and bed temperature, and tested in the same way on the same hydrostatic tester, and with the exception of the initial thinning and then addition of the 5AAM G-code sections, are printed from the same G-code. A typical specimen failure can be seen in figure 7; the test ABS is red, and the translucent material is the latex membrane used for waterproofing.

Figure 7: Typical failure mode of a hemispherical dome.

We excluded all failed or defective prints (prints that were visibly defective or failed when we tried to remove them from the print bed). We also noted a distinct variation in weight – specimens made in 5AAM modes were usually slightly less massive than conventional 3D

printing. Although the 5AAM parts were dimensionally acceptable, they were clearly less dense (sometimes up to 25% less dense) – meaning that the 5AAM G-code our interim script was generating was not exactly correct, or perhaps our extruder hardware was not up to the task of precise extrusion amounts during the varying back-pressure of 5AAM printing; after a good cleaning, the masses of both kinds of parts increased, so this may have been due to coking in the nozzle. In any case, the specimen masses were consistently within a range of 50 milligrams for any particular G-code (control disk, conventional 3D dome, or 5AAM dome) and nozzle state. From the results in this table, we may reasonably conclude that:

- Conventional 3D printing is demonstrably weak in Z, by roughly a factor of two. (none of the conventional 3D printed domes reached the strength level of even the weakest flat disk).
- 5AAM printed domes of the same shape were both lighter and much stronger than both the conventionally printed flat disk and the conventionally printed 3D domes. The 5AAM process, which changed only the G-code and nothing else, produced ABS parts with roughly a 4.5x increase in strength to weight ratio.
- The weakest 5AAM part was stronger than the strongest part produced by any conventional 3D printing method or CAD design.

This is a strong validation of the original hypothesis: orienting the lay-down paths in the direction of stress yields stronger parts.

However, it opens the question of whether this result is applicable only to the ABS styrene copolymer or whether it applies to other polymers as well.

Experimental Results II: To resolve this uncertainty, we then repeated the conventional dome versus 5AAM dome test set using two additional polymers – nylon 645 (“Bridge”) which is a polyamide, and FDA-approved “T-glase” polyester (both supplied by Taulman3D). As the nylon 645 is somewhat hygroscopic, we stored it over silica gel in a desiccator when not in use; this minimized the steaming and bubbling that others have reported while using nylon for FFF fabrication. The T-glase polyester was stored in normal (air-conditioned) office conditions.

Unfortunately, we were unable to achieve sufficient temperatures in our long-reach 5AAM extruder as the extruder uses a thermal break made of PEEK (polyetheretherketone) in a structural role. At the temperatures and stresses needed to extrude nylon 645 and T-glase, the PEEK softens and (to our chagrin) fails catastrophically.

Reconsidering our options (and remembering that our specimen base-to-dome angle is 45 degrees), we modified a spare Lulzbot TAZ all-metal hotend to extend the clearance cone of 45 degrees to the full height of our specimen dome needed during printing – approximately 11 mm. This entailed relocating cooling fans and grinding away part of the heater retention metal, but gave us a 3-degree-of-freedom printer that the manufacturer rates to operate up to 300degC. This extruder uses a stainless steel thermal break and thus requires an active cooling fan, but it does operate correctly at these temperatures.

We then performed the same dome experiment as above, but with nylon 645 and T-glase polyester. The results are shown in Table 2.

We should note that even with the modified all-metal extruder, we still had considerable difficulty printing T-glase domes due to the very far overhang involved. We slowed the print speed to 1/3 of normal and still had a large fraction of failed prints (prints that were visibly defective, usually as failed dome cantilevering during the printing process). As in experiment series 1 in ABS, we excluded any part that had visibly failed before the start of pressure testing from this table.

Table 2: Nylon 645 and T-glase polyester strengths:

Shape	**Nylon 645 Conventional 3D dome**	**Nylon 645 5AAM process**	**T-glase polyester conventional 3D dome**	**T-glase polyester 5AAM process**
Average Rupture Pressure in MPa	1.12 MPa	4.46 MPa	1.22 MPa	3.95 MPa
Individual Specimen Rupture Pressure in MPa	0.1 0.1 0.4 1.5 3.5 $\sigma^2 = 1.68$	4.05 4.1 4.1 4.3 4.35 5.9 $\sigma^2 = 0.42$	0.2 0.8 1.6 1.6 1.9 $\sigma^2 = .39$	2.2 2.95 3.0 5.3 5.3 $\sigma^2 = 1.68$
Strength/weight ratio in MPa / gram	0.132	0.607	0.138	0.446
5AAM advantage in Z (S/wt)		**4.59 x stronger**		**3.23 x stronger**

Like the experimental results for ABS, we see that nylon and polyester show a strong improvement in strength to weight ratio; >4.5x for nylon, and >3.2x for polyester, from the same spool of the same material printed on the same machine at the same extruder temperature and bed temperature.

Discussion and Conclusions: Given the experimental results (strength to weight ratios of ~3x to 5x higher, while building from the same CAD model, with the same spool of polymer on the same machine at the same extruder and bed temperatures) we feel justified in concluding that the hypothesis is proven, that it *is* possible to make strong parts in FFF just by changing the lay-down paths so that the lay-down paths align with the direction of stress in the part.

Further, we found that the strength increase is not idiosyncratic with respect to ABS copolymer, but also applies to nylon polyamides and T-glase polyesters.

We noted that without exception, that even the weakest 5AAM part was stronger than the strongest conventionally-made part made of the same spool of the same polymer with the same processing conditions.

We also found that for CAD models that the nozzle can reach mechanically without crashing the nozzle into the partially built part, that a full 5-axis articulation may be unnecessary, and some significant and useful part shapes can be printed with stress-tensor-aware G-code on either unmodified 3-axis printers, or 3-axis printers with only trivial modifications to increase nozzle clearance.

Finally, we found that 5AAM specimens had a much lower risk of being “crypto-defective” – that is, a specimen that passes external visual inspection, but that fails at a very low loading. We intentionally excluded from consideration the data on any test specimen that we could see was visually defective before applying test pressure, but kept those specimens that showed no visual abnormalities even if their test to destruction values showed a very low strength (indicating a crypto-defective specimen). In other words, to avoid “cherry-picking” data, once we started to test a specimen., we committed to report that specimen’s data in the results, no matter how high or low the value was.

Retrospectively, we did test some visually rejected specimens (failed builds, not included in the statistics above, usually where the inner dome cantilever hand collapsed downward, partially filling the dome with loose extrusion). We did this out of a sense of curiosity to observe their failure modes and were surprised that some of these obviously bad 5AAM specimens still had strength-to-weight ratios stronger than the strongest conventional parts, even though a considerable mass fraction of polymer was unconsolidated loose extrusion that could easily be moved around with the fingertips. We did not include these visually rejected specimens in the above statistics, even though they would have improved our strength-increase values.

Criticisms and Further Research Directions: Although 5AAM can create parts of outstanding strength, the process is not without engineering challenges.

First; the 5AAM process is considerably slower than conventional printing, partially because of the slow A and B axis planetary reduction gearboxes at 51:1 gear reduction and anti-backlash spring preloading. A precise yet fast angular rotation platform is needed (or an alternative, such as a six-linear-strut hexapod (a.k.a. “Stewart platform”) or even a 6- or 7-DoF polar robotic arm, if sufficient positional accuracy can be obtained (better than 25 microns). Our software could also optimize feedrates and do better at segment merging.

Second, design of extruder hot-end nozzles is still an area of active research.. Adding the additional constraint of a long reach and a small included angle makes the problem even more difficult. Our experience led to several heater/nozzle failures in use. In the future, it may be appropriate to use an actively cooled nozzle support (either air or water-cooled, with a stainless-steel or even a ceramic thermal break). Some observers indicated that a long melt zone causes subsequent difficulties such as nozzle coking and protracted drooling or thread depositing; our current design has a melt zone of nearly 30mm, which is considered very long,

Third, our choice of a delta machine over a tip-tilt table gives a very tall machine with only a small build volume; it works well for initial research because of the easy access and modification, but for production use it is inefficient, and other systems may be better alternatives.

Fourth, we have not yet evaluated 5AAM with composite materials, such as polymers with chopped fibers such as graphite or Kevlar strands embedded in the mix.

Video: A video of the process may be seen at [6] showing the 5AAM printer in operation. Alternatively the title is “Five Axis Additive Manufacturing”, available on YouTube.

References:

[1] A Sherif El-Gizawy, Shan Corl, Brian Graybill, whitepaper, “Process Induced Properties of FDM Materials”, University of Missouri Mechanical and Aerospace Engineering Department

[2] Ivan Gajdos, Jan Slota, “Influence of Printing Conditions on Structure in FDM Prototypes” Technical Gazette, ISSN 1330-3651 / 1848-6339, Technical University of Kosice, Slovak Republic

[3] Sung-Hoon Ahn, Michael Montero, Dan Odell, Shad Roundy, Paul K. Wright, “Anisotropic Material Properties of Fused Deposition Modeling ABS”, Rapid Prototyping vol 8 nr 4 2002 ISSN 1355-2546

[4] Constance Ziemian, Mala Sharma, Sophia Ziemian, “Anisotropic Mechanical Properties of ABS Parts Fabricated by Fused Deposition Modeling”, ISBN 978-953-51-0505-3, InTech open science, www.intechopen.com.

[5] Øyvind Kallevik Grutle, “5 Axis 3D Printer”, Master’s thesis, University of Oslo.

[6] https://www.youtube.com/watch?v=Fomi0V_xl4k